Percolation Effects in Electrolytically-Gated WS_2/Graphene Nano:Nano Composites

Domhnall O'Suilleabhain,[#,1,2] Victor Vega-Mayoral,[#,1,2] Adam G. Kelly,[#,1,2] Andrew Harvey[1,2] and Jonathan N. Coleman[*1,2]

[1]*CRANN & AMBER Research Centers, Trinity College Dublin, Dublin 2, Ireland*

[2]*School of Physics, Trinity College Dublin, Dublin 2, Ireland*

[#] *Equally contributing authors*

[*]colemaj@tcd.ie (Jonathan N. Coleman); Tel: +353 (0) 1 8963859.

ABSTRACT: Mixed networks of conducting and non-conducting nanoparticles show promise in a range of applications where fast charge transport is important. While the dependence of network conductivity on the conductive mass fraction (M_f) is well understood, little is known about the M_f-dependence of mobility and carrier density. This is particularly important as the addition of graphene might lead to increases in the mobility of semiconducting nanosheet-network transistors. Here, we use electrolytic gating to investigate the transport properties of spray-coated composite networks of graphene and WS_2 nanosheets. As the graphene M_f is increased, we find both conductivity and carrier density to increase in line with percolation theory with percolation thresholds (~8 vol%) and exponents (~2.5) consistent with previous reporting. Perhaps surprisingly, we find the mobility increases modestly from ~0.1 cm^2/Vs (for a WS_2 network) to ~0.3 cm^2/Vs (for a graphene network) which we attribute to the similarity between WS_2-WS_2 and graphene-graphene junction resistances. In addition, we find both the transistor on- and off-currents to scale with M_f according to percolation theory, changing sharply at the percolation threshold. Through fitting, we show that only the current in the WS_2 network changes significantly upon gating. As a result, the on-off ratio falls sharply at the percolation threshold from ~10^4 to ~2 at higher M_f. Reflecting on these results, we conclude that the addition of graphene to a semiconducting network is not a viable strategy to improve transistor performance as it reduces the on:off ratio far more than it improves the mobility.

Keywords: Printed electronics, thin film transistor, graphene, WS_2, composite, ionic liquid, carrier density, mobility.

Introduction

Over the last few years, advances in solution processing have facilitated the mixing of various combinations of nanomaterials, allowing the investigation of hitherto inaccessible composite materials.[1] Such mixtures are often referred to as nano:nano composites and differ greatly to standard nanocomposites.[2] Nano:nano composites can, for example, be extremely porous which lends them to specific applications such as electrochemical devices where the electrolyte can be introduced into the pore volume.[3] These composites can also be composed of mixed dimensionalities leading to useful combinations of properties; the addition of a small amount of carbon nanotubes to an MoS_2 nanosheet network results in very large improvements in electrical conductivity as well as mechanical toughness.[2] It has also been shown that the lithium storage capacity of silicon nanoparticles can be maximised via the addition of small amounts of graphene to increase the electrode conductivity.[4] Such graphene-silicon nanoparticle composites combine zero-dimensional and two-dimensional materials and are labelled 2D:0D nano:nano composites. Recently, a number of papers have reported composites of various combinations of dimensionalities such as 2D:2D,[5-7] 1D:2D,[8-10] 2D:0D,[11-12] and 1D:0D.[13-14] These composites have been utilised in a range of applications such as transparent conducting coatings,[15] energy storage devices[8-10] and photo/electro-catalytic systems.[16-18]

In stark contrast with other types of composite, the basic properties of these nano:nano composites are still not well studied. Many of the nano:nano composite applications involve improving the conductivity of one nanomaterial through the addition of a second conducting nanomaterial (e.g. graphene or carbon nanotubes). While a number of papers have studied how the resultant composite conductivity scales with the loading level of the conductor, and analysed the results using percolation theory, to the author's knowledge no papers have gone beyond this. It is therefore not known how basic quantities such as mobility and carrier density scale with volume fraction in such composites (in fact, very few papers have measured these properties, even in the more well-known polymer-based nanocomposites[19-20]).

This lack of information about mobility and carrier density in nano:nano composites is a barrier to the development of these materials in new applications. We have previously suggested, based on photoconductivity data, that the mobility of 2D:2D composites might increase significantly upon the addition of graphene nanosheets.[21] This would be an important development which would be of use in the area of printed electronics using 2D materials.[22-26] A number of papers have described printed electronic devices such as photodetectors,[21] switches,[23] memory elements[25] and transistors[22, 27] which are predominately based on networks of 2D nanosheets. However, nearly all such devices are limited by relatively low mobilities

which tend to be ~0.1 cm^2/Vs for printed networks of transition metal dichalcogenide nanosheets.[27] If, as suggested,[21] the addition of graphene to a semiconducting nanosheet network does indeed increase the mobility, this would represent a very simple way to enhance the mobility in such devices. On the other hand, if the addition of graphene does not enhance the mobility in such networks, it would still be important to understand how carrier density and mobility depend on conductor content as this information will shed light on the factors limiting carrier transport.

In this work, we fabricated a set of nano:nano composites based on mixtures of WS_2 and graphene nanosheets. We measured the electrical conductivity as a function of graphene content both before and after an ionic liquid was added to the network. The presence of an ionic liquid coupled with the addition of a gate electrode allows the system to function as an electrolytically-gated transistor. The analysis and fitting of the transfer curves yields the mobility which is then assessed as a function of graphene content. Combining conductivity and mobility yields the carrier density, thus giving a complete description of how the primary conductivity parameters depend on graphene content. In addition, this work also sheds light on the performance of electrolytically gated transistors based on 2D:2D composites.

Results & Discussion

Materials and network formation

Both WS_2 and graphene powders were produced by liquid phase exfoliation[28] via sonication in the solvent N-Methyl-2-pyrrolidone (NMP) followed by centrifugation to optimise the nanosheet size distributions by removing very thin nanosheets which tend to have thickness-dependent bandgaps[29] (Methods). To facilitate deposition, the nanosheets were transferred to isopropanol (IPA) prior to deposition. This process yielded graphene and WS_2 inks as shown in the inset of Figure 1A.

Extinction spectra measured on these inks are plotted in Figure 1A. The main spectral features of WS_2 are clearly visible such as the A-exciton at ~630 nm.[29-30] It has been shown that the A-exciton position can be used to estimate the mean nanosheet thickness in suspended ensembles.[29] This method is thought to be reasonably accurate, giving mean nanosheet thicknesses which are accurate to within a monolayer or so. Analysis of the data in Figure 1A yields a mean thickness of ~9 monolayers per WS_2 nanosheet. This fulfils our main thickness-

requirement which is to predominately obtain nanosheets with more than 6 monolayers to avoid variations in bandgap for nanosheets of different thicknesses.[31]

The graphene spectrum exhibits a flattish plateau at high wavelength with the characteristic Van Hove singularity present at ~300 nm.[32] From the ratio of extinction at 550 nm to that at 325 nm, we estimate the mean nanosheet thickness to be ~12 monolayers.[33] We also performed a comprehensive TEM analysis in the nanosheets found in both inks with sample images shown in the insets of Figures 1B and C. The nanosheet length distributions are plotted as histograms in Figures 1B and C and show the expected lognormal distribution with average lateral lengths of 470 and 680 nm for WS_2 and graphene, respectively.

Inks such as those described above can easily be formed into films through spray coating. Here we sprayed a range of films from both the graphene and WS_2 inks as well as from composite inks formed by mixing the WS_2 and graphene inks in various ratios. Deposition of such composite inks results in the formation of composite films formed from mixtures of WS_2 and graphene nanosheets at various graphene mass fractions, M_f ($M_f = M_{Gr} / (M_{WS_2} + M_{Gr})$).

To investigate the electrical behaviour of these composites, gold electrodes were deposited on top of the sprayed network by evaporation. Shown in Figure 1D is a representative SEM image of a typical WS_2-graphene composite network showing the interface between the electrode and the network. The film clearly consists of a disordered array of nanosheets. This image also shows the gold contact follows the topography of the rough surface of the film, suggesting an intimate contact. The randomness of the nanosheet alignment means the film is not densely packed, with previous work having shown such networks to have a porosity of ~40-60%.[2, 27] Such a large internal free volume allows nano:nano networks such as these to be filled with electrolyte or ionic liquid (IL) facilitating a number of applications such as battery[10] or supercapacitor[2] electrodes, solar cells[34] and sensors.[35]

These composite networks can be characterised further using Raman spectroscopy which can be used to confirm the quality of the material after deposition and to assess the distribution of the graphene in the composites. Figure 1E shows a representative Raman spectrum from the M_f=0.5 network which shows modes from both WS_2 (E_{2g} and A_{1g}) and graphene (D, G and 2D). As the intensity of the Raman signal depends on the quantity of material under illumination, the relative intensities of WS_2 and graphene modes will vary with M_f. This will be valid so long as the films thicknesses are roughly constant (as is the case here) and the surface morphology (e.g. roughness and uniformity) are similar across all mass fractions. We expect the latter point to be approximately true because the similarity in dimensions between

the WS_2 and graphene nanosheets should result in M_f-independent network structure. It was previously shown that the intensity ratio of any WS_2 mode (e.g. E_{2g}) to that of any graphene mode (e.g. the G band) should scale linearly with the WS_2-to-graphene mass ratio as [2, 36]:

$$\frac{I_{E_{2g}}}{I_G} \propto \frac{M_{WS_2}}{M_{Gr}} = \frac{1}{M_f} - 1. \quad (1)$$

where I_{E2g} and I_G are the intensities of the WS_2 E_{2g}-mode and the graphene G-mode, respectively. As shown in Figure 1F, we find the expected scaling which indicates that the average composite composition scales with mass fraction. However, we note that Raman mapping (see SI) showed the graphene to be not perfectly homogeneously dispersed with some clumping observed, an issue which is quite common in nanocomposites.

While the constituents of such composites are often described in terms of mass fraction, the composite properties are always analysed in terms of volume fraction, ϕ. In nano:nano composites it is especially important to include porosity when converting M_f to ϕ. With this in mind, the graphene volume fraction can be expressed as:[2]

$$\phi = \frac{(1-\phi_P)}{1+\frac{\rho_G}{\rho_{WS_2}}\frac{1-M_f}{M_f}} \quad (2)$$

where ϕ_P is the porosity (the fraction of pore volume) and ρ_G =2200 kg/m^3 and ρ_{WS_2} = 7500 kg/m^3 are the graphene and WS_2 densities, respectively. Here, we assume ϕ_P =0.5, as porosities of 0.4-0.6 have been reported for a range of solution-processed nanosheet networks.[27] We assume ϕ_P is roughly independent of M_f because the network porosity should be predominately determined by nanosheet dimensions. As both nanosheet types have similar sizes and thicknesses, we do not expect significant variations in porosity with M_f. We further justify this by noting that detailed measurements on MoS_2/SWNT nano:nano composites showed porosity variations of no more than 5% from the mean over the whole compositional range.[2] Assuming ϕ_P =0.5, WS_2-only networks are represented by ϕ =0, while ϕ =0.5 represents a graphene-only network.

Electrolytic gating: TFT characterisation

We performed a full volume-fraction-dependent electrical characterisation of WS_2-graphene composites including WS_2-only and graphene-only networks. The conductivity of the as-produced networks was measured in the "dry" state i.e. before filling the porous interior with

ionic liquid to facilitate mobility measurement through electrolytic gating. The conductivity was then measured in the "wet" state i.e. after ionic liquid addition. In addition to conductivity, in the wet state we can obtain data on mobility and carrier density as well as electrolytically gated transistor data, all as a function of graphene volume fraction.

The device fabrication and characterisation protocols are described in detail in the methods section where the process follows that reported in Ref[27]. Figure 2A shows a schematic of an electrolytically gated nanosheet-network transistor while a photograph of the electrode array is given in Figure 2B. When a voltage is applied to the gate electrode, ions of a given charge are driven to the nanosheet-IL surfaces within the porous interior of the network. This results in electrons/holes being drawn into the nanosheet network to compensate the ionic charge leading to accumulation mode behaviour.

Figure 2C shows output curves (drain-source current, I_{DS}, as a function of the drain-source voltage, V_{DS}) for films with graphene mass fractions ranging from 0 wt% (WS_2-only) to 100 wt% (graphene-only). These output curves are measured in the "dry" state, i.e. prior to addition of the ionic liquid, and show the expected increase in conductance with graphene content. Figure 2D shows the same measurements in the "wet" state, i.e. after the addition of the ionic liquid. Here we see the addition of the ionic liquid causes an increase in the zero-gate-voltage conductivity, especially at low M_f. This has previously been observed and may be caused by the non-uniform distribution of ions at the basal planes of the nanosheets causing localised carrier accumulation.[27]

Figure 2E shows the family of transfer curves (drain-source current, I_{DS}, as a function of the gate voltage, V_G) for a range of nano:nano composite networks with M_f ranging from 0 wt% to 100 wt%. This graph clearly demonstrates the channel transition from semiconducting (low M_f) to semimetallic (high M_f), with the suppression of the on:off ratio associated with the increasing off-currents shown in Figures 2C and D. The transfer curve of the ϕ=0 TFT (Figure 2F) shows a high on:off ratio (~10^4) and relatively low on-current (~1 mA). This is a significantly higher on:off ratio than in our previous report[27] and is due to refinement in the measurement technique where a dynamic I_{DS} range was used, instead of a fixed I_{DS} range or autorange, allowing us to better characterize both I_{on} and I_{off}. The transfer curve of the graphene-only TFT (ϕ=0.5, Figure 2G) is typical of a semi-metal, with an on:off ratio below 2 and much larger on- and off-currents.

It is clear from the data in Figure 2 F-G that application of a given gate voltage has a much greater relative effect on the WS_2-only film compared to the graphene-only network. We

believe this is simply due to the fact that graphene has a much larger carrier density than WS_2 in the absence of gating. Application of a gate voltage should induce a carrier density of $\sim C_V V_G$ where the volumetric capacitance of the network, C_V, depends on the nanosheet thickness.[37] As the WS_2 and graphene nanosheet have very similar thicknesses, we expect the induced carrier densities to be similar for all compositions. This will result in a much greater relative change in current for WS_2 networks, which have much lower charge densities to start with.

The results of the electrolytic gating experiments are shown in more detail in Figure 3. The "wet" electrical conductivity (measured at $V_G = 0$ V) of the nanosheet network in the presence of IL generally increases with graphene content as shown in Figure 3A. Despite a slight apparent fall-off in conductivity at low mass fractions, the conductivity undergoes a sharp thousand-fold increase between ϕ=0.08 and 0.11, followed by a more gradual increase thereafter. This is consistent with percolation theory[38] which predicts a sharp increase in conductivity at the percolation threshold, the volume fraction where the first continuous conductive network appears (see below for more detailed analysis). Above ϕ~0.25, the network characteristics are completely dominated by the graphene and the conductivity saturates at a value of ~500 S/m.

As was shown in Figure 2C and D, the conductivities in the presence of the IL are much larger than those in the dry state. The ratio of wet:dry conductivity is shown in the inset of Figure 3A. This ratio is ~1000 for the WS_2-only network but falls off rapidly with ϕ, reaching ~1 at ϕ~0.08. It is likely that the presence of IL results in inadvertent doping of the WS_2, perhaps due to an imbalance in the cationic and anionic population at the nanosheet basal planes even in the absence of gating. As the graphene nanosheets have a much higher carrier density than those of WS_2, this effect should fall with ϕ. Indeed, we would expect it to disappear at the percolation threshold where conduction becomes dominated by the graphene, in line with observations. Such inadvertent doping has already been observed in MoS_2, WS_2, $MoSe_2$ and WSe_2 TFTs (see ref[27] SI). In agreement with the suggestion above, for those materials the relative increase in conductivity, once the IL is added, is lower in those materials with larger density of charge carriers (WSe_2 in that case).

The evolution of both on-current (current at V_G = -2.5 V) and off-current (minimum current) with ϕ is shown in Figure 3B. At low ϕ, the off-current is relatively small, ~0.1 μA, but undergoes a sharp increase at ϕ~0.07 before increasing more gradually in a manner similar to

the data in Figure 3A. The on-current behaves in a similar manner, although starting from a much higher value at low ϕ.

We explain this behaviour using percolation theory which can be used to describe the conductivity of conductor/insulator mixtures. Within this framework, as the conductor volume fraction is increased the conductivity first increases slowly until the percolation threshold – the volume fraction where the first continuous conductive path is created – is reached, after which the conductivity increases rapidly. Although effective-medium models can describe the conductivity versus volume fraction data over the whole ϕ-range,[38] it is generally simpler to use separate equations for the conductivity above and below the percolation threshold. Above the percolation threshold, the conductivity is often written as:

$$\sigma = \sigma_0 \left(\phi - \phi_c\right)^n \tag{3a}$$

where σ_0 is a constant related to the conductor conductivity, ϕ_c is the percolation threshold and n is the percolation exponent. However, we have pointed out[39] that in electrochemical devices, the insulator (here, WS_2 in the wet state) conductivity cannot be neglected and the data fits well to

$$\sigma = \sigma_{Ins} + \sigma_0 \left(\phi - \phi_c\right)^n \tag{3b}$$

where σ_{Ins} is the insulator conductivity and can be thought of as representing the contribution to the conductivity of current flowing through the WS_2-only sub-network. Due to the proportionality between current and conductivity, we propose that this equation can be used to describe the current flowing in both the on and off states. Rewriting this equation to describe the current data in Figure 3B yields

$$I_{\text{on}} = I_{\text{on,WS2}} + I_{\text{on,Gra}}\, 2^n \left(\phi - \phi_c\right)^n \tag{4a}$$

and

$$I_{\text{off}} = I_{\text{off,WS2}} + I_{\text{off,Gra}}\, 2^n \left(\phi - \phi_c\right)^n \tag{4b}$$

where we treat the on and off states separately. In these equations, the factor of 2^n accounts for the fact that the graphene-only film occurs at ϕ=0.5. Fitting both on- and off-current data to these equations yields $I_{on,WS2}$=1.3 mA, $I_{on,Gra}$=130 mA, ϕ_c=0.08 and n=2.6 for the on-state and $I_{off,WS2}$=0.1 μA, $I_{off,Gra}$=76 mA, ϕ_c=0.08 and n=2.5 for the off-state.

Figure 3C shows the on:off ratio plotted as a function of graphene volume fraction. As in Figure 3B, we can identify two regimes of behaviour either side of the percolation threshold (ϕ_c=0.8).

Below the percolation threshold, the on:off ratio is roughly constant at ~10^4. This contrasts sharply with the post-percolation regime where the current flows predominantly through the graphene sub-network and the I_{on}/I_{off} falls sharply, approaching 1.5 for loading levels above ϕ=0.08. The data in Figure 3C can be described by a combination of Equations 4A and 4B:

$$\frac{I_{on}}{I_{off}} = \frac{I_{on,WS2} + I_{on,Gra}\, 2^n \left(\phi - \phi_c\right)^n}{I_{off,WS2} + I_{off,Gra}\, 2^n \left(\phi - \phi_c\right)^n} \tag{5}$$

This function is plotted in Figure 3C using the fit parameters described above but using n=2.5 in both denominator and numerator. From these fit parameters, we can estimate the on:off ratio for WS_2-only and graphene-only networks as $(I_{on}/I_{off})_{WS2}=1.3\times10^4$ and $(I_{on}/I_{off})_{Gra}=1.7$.

The model described above confirms that electrolytic gating modulates the conductivity of WS_2 and graphene nanosheets to vastly different degrees as discussed above. The properties of the composite network are given by a combination of both sub-networks as described by percolation theory. As a result, the switching properties of 2D:2D composite TFTs are strongly influenced by percolation theory and are quite sensitive to the percolation threshold. However, it is clear from the fit parameters above that the electrical properties of the WS_2 nanosheet are much more sensitive to gate activation and it is those properties which dominate the switching behaviour of the composite at all graphene loadings, especially below the percolation threshold.

In general, although the conductivity increases significantly with graphene content, it is not clear whether this is due to changes in carrier density, mobility or both. Photoconductivity measurements in MoS_2-graphene composites have suggested that mobility and carrier density are affected more or less equally[21] while Hall effect measurements on polymer-nanotube composites have suggested that it is solely the carrier density that is affected by the addition of a conductor.[19]

For electrolytically gated nanosheet networks, the mobility can be found using the following equation:[27]

$$\frac{\partial I_{DS}}{\partial V_G} = \mu C_V t \frac{w}{l} V_{DS} \tag{6}$$

where C_V is the volumetric capacitance of the network, t is its thickness and the other symbols have their usual meaning. For each transfer curve (I_{DS} versus V_G), there is a linear region where $\partial I_{DS} / \partial V_G$ can be found by fitting. In all cases, fitting was carried out on the "p" side of the transfer curve so all μ-values are hole mobilities. It is then possible to obtain the volumetric capacitance-mobility product, μC_V, as the figure of merit for such transistor systems. This

parameter is plotted versus ϕ in Figure 3D and shows only a small variation from 0.1 to 0.6 $Fcm^{-1}V^{-1}s^{-1}$ over the entire ϕ-range. To extract μ, we measured the volumetric capacitance for a subset of volume fractions, calculating the remaining values through interpolation (SI). The resultant mobility data is plotted versus ϕ in Figure 3E. The mobility increases steadily with increasing graphene content from 0.11 $cm^2\ V^{-1}\ s^{-1}$ for the WS_2-only network to 0.35 $cm^2\ V^{-1}\ s^{-1}$ for the graphene-only channel.

The WS_2-only mobility is broadly in line with previous results.[27, 40] However, the graphene value is much lower than the reported (electrostatically gated) mobilities for inkjet-printed graphene networks.[22, 26] This discrepancy can likely be attributed to morphological differences between inkjet-printed and sprayed networks which lead to different distributions of inter-nanosheet junctions, leading to higher junction resistances and lower mobilities in the networks reported here. For example, basal plane-basal plane junctions would be expected to have much lower resistances than plane-edge or edge-edge junctions. It is likely that inkjet printing and spraying give different populations of the various junction types, resulting in large mobility variations. Indeed the dry conductivity of the graphene-only network reported here was 300 S/m, roughly ×70 lower than typical graphene networks.[41] This is consistent with the graphene networks fabricated here having lower than normal mobility. In addition, this idea is supported by a recent report by Lin *et al.*[42] which showed a highly aligned MoS_2 network with predominately plane-plane junctions to have a very high mobility of ~5-10 cm^2/Vs. This strongly highlights the importance of optimising network morphology for electronic devices. The low mobility found here may also be compounded by the lack of an annealing step during device fabrication. The performance of the WS_2 devices was found to decline after an annealing step (SI) and hence was omitted from our fabrication protocol.

High performance transistors require high values of both the mobility and on:off ratio. However, as shown in Figure 3F, these two parameters are negatively correlated in these 2D:2D composites meaning the improvement of one leads to a reduction in the other. Thus, the addition of graphene to semiconducting nanosheet networks does not appear to be a valid strategy for improving transistor performance.

A key strength of electrolytically gated TFTs is their low voltage operation made possible by the high capacitance associated with the double layer. One way to characterise the operating voltages is via the threshold voltage. The threshold voltage can be found using the same linear regression used to obtain $\partial I_{DS} / \partial V_G$ in Equation 6 and Figure 4A plots the threshold voltages,

V_{th}, extracted from the transfer curves for each composite for both p- and n-regions. In both cases, the threshold voltage decreases strongly with increasing ϕ. The difference in n and p threshold voltages, ΔV_{th}, is plotted versus ϕ in Figure 4B. This parameter has been associated with the electrical bandgap, especially in electrolytically gated devices where the capacitance is high.[43-44] While Figure 4B implies a bandgap of ~3 eV for the WS_2-only network, this value is relatively high compared to the reported optical bandgap of ~2 eV for bulk WS_2.[45] While some of this difference may be attributed to an exciton binding energy of ~0.5 eV[46-48], it is likely that the obtained value of 3 eV contains significant inaccuracy due to hysteresis effects which are omnipresent in electrolytically gated TFTs.[49] Interestingly, ΔV_{th}, falls with increasing volume fraction scaling in proportion to ϕ^{-1}. While the reason for this particular ϕ-dependence is unclear, it is likely that ΔV_{th} represents an effective bandgap which approaches zero for the graphene-only network.

We complete the transistor analysis by measuring the temporal current response to a step increase in gate electrode from V_G = 0 V to -2.5 V for a subset of volume fractions. As shown in Figure 4C, the WS_2-only network shows a relatively slow response with the current increase becoming more rapid with increasing graphene content. These non-instantaneous responses are due to the non-negligible time taken for both ions and electronic charge carriers to respond to the gate voltage. Adding graphene to the composite increases the electrical conductivity and reduces the time taken for gate-induced carrier accumulation to occur. These data are best fitted by a bi-exponential expression where two lifetimes have been extracted from the fits (Figure 4D). Each of these lifetimes shows a similar evolution with ϕ suggesting that both are affected by the electronic conductivity of the network. We hypothesise that the presence of two characteristic times is related to the ionic diffusion under a gate potential. In ionic liquids, the electric double layer is composed of 2 sublayers; the first is a densely packed layer of ions that are strongly adsorbed at the interface, and the second is a diffuse outer layer characterised by a monotonic, long-range attraction.[50] This second interaction is rather weak as the surface charge is strongly screened by the compact surface layer resulting in a delayed interaction with the diffuse layer. We thus posit that the interplay between these two ionic layers is the origin of the two lifetimes present in the temporal data.

Electrical properties of 2D;2D composites

We can use the electrolytically gated transistor characterisation described above to assess the dependence of the conductivity, mobility and carrier density on ϕ in these 2D:2D composites. The composite electrical properties in the presence of ionic liquid, as described above, are useful in the context of electrolytic devices. However, from a materials characterisation perspective, it is the properties of the dry networks (never having been exposed to ionic liquid) which are most relevant. Shown in Figure 5A is the dry electrical conductivity, extracted from Figure 2C, plotted versus ϕ. This data has been fitted to percolation theory using Equation 3A (as we expect σ_{Ins} to be small in the dry samples), with the percolation plot shown in the inset. Fitting yielded σ_0=9000 S/m, ϕ_c=0.09 and n=2.5. We note that the latter two parameters are very similar to those found for the wet networks shown in the Figure 3B fits. This is as expected as both these parameters[38] are associated with either the nanosheet properties[36] (ϕ_c) or the structure of the emerging graphene network[2] (n) and should be insensitive to the presence or absence of ionic liquid. We note that the percolation threshold is quite high compared to values of <1% often reported in polymer-graphene composites.[51] However, the values reported here are consistent with values of >10% found previously in graphene-filled nano:nano composites. Such large values are expected where the graphene sheets are largely oriented in-plane.[36]

While the dependence of conductivity on conductor loading level has been reported for a number of nano:nano composites,[2, 52] to our knowledge mobility and carrier densities have never been directly measured as a function of loading level. In fact, mobility and carrier density values have hardly ever been reported, even for polymer-based nanocomposites, a very heavily studied class of materials.

To address this deficit, we assume that the network mobility is not significantly impacted by the presence of ionic liquid. This allows us to approximate the dry mobility from the mobility measured in the presence of the ionic liquid, shown in Figure 3E. Such an approximation has been previously demonstrated[53] and can be explained by noting that the addition of ionic liquid is expected to predominately affect the carrier density through residual doping due to unbalanced interfacial ionic populations even in the absence of gate voltage. We expect the mobility to be limited by junction resistances in such nanosheet networks.[54-55] While junction resistance may be modified by the effect of ionic liquid on inter-sheet tunnelling, we expect this to be a relatively small effect. Indeed, if junction resistances (and hence network mobility) were significantly modified by the presence of IL, we would expect the graphene-dominated networks (ϕ=0.5) to show significant conductivity differences between dry and wet states as the graphene networks are heavily junction limited due to the low resistance of the nanosheets.

Conversely, under these circumstances, the WS_2-dominated networks (below the percolation threshold) should be less impacted by the presence of IL because the high inter-sheet resistance makes the junctions less important. This is the opposite of what is observed in Figure 3A (inset), strongly implying the addition of IL enhances the effective carrier density.

The discussion above allows us to use the mobility in the presence of ionic liquid as an approximate representation of the intrinsic hole mobility of the dry network (as shown in Figure 5B). This mobility changes very little with graphene content, changing only by ×3 over the entire compositional range. However, it undergoes an increase in the vicinity of the percolation threshold (ϕ~0.08) before largely saturating above ϕ~0.2. Such a small variation cannot be explained by differences in intrinsic intra-sheet mobility. Rather, we believe this is a manifestation of small differences in tunnelling resistances at WS_2-WS_2, WS_2-graphene and graphene-graphene junctions. Below the percolation threshold, charge transport is predominately via WS_2-WS_2 junctions while at high ϕ-values graphene-graphene junctions are dominant. We can model the network conductivity by noting that transport is a combination of intra-sheet transport accompanied by inter-sheet tunnelling. This means that current paths are made up of a series of nanosheet resistance/junction resistance combinations. This allows us to model the network mobility, μ, via the contributions from nanosheet mobility, μ_{NS}, and inter-nanosheet tunnelling (represented by μ_{Jun}):

$$\frac{1}{\mu} = \frac{1}{\mu_{NS}} + \frac{1}{\mu_{Jun}} \qquad (9)$$

For both graphene and WS_2, the nanosheet mobility is much larger than the values of μ presented in Figure 5B, allowing us to approximate $\mu \approx \mu_{Jun}$, i.e. that network mobility is dominated by junctions in all cases. Then, comparing the low-ϕ mobility data to the data for $\phi \rightarrow 0.5$ implies the graphene-graphene junction resistance to be ~×3 lower than the WS_2-WS_2 junction resistance.

We can combine the "dry" conductivity and hole mobility data shown in Figures 5A and B to yield an effective "dry" hole density for WS_2-graphene composites as shown in Figure 5C. In each case, the data has been expressed on a per unit area of nanosheet basis by correcting for network porosity and nanosheet thickness. Here we see a significant increase from ~10^8 cm^{-2} for the WS_2-only network to ~10^{14} cm^{-2} for the graphene-only network. The latter value is consistent with reported levels for graphene (10^{13}-10^{15} cm^{-2}),[56-57] however, the density of charge carriers in the WS_2-only network is 5 orders of magnitude lower than those reported for

a heavily doped few-layer WS_2 transistor (10^{13} cm^{-2}).[43] Interestingly, because of the small variation in mobility with graphene content, the carrier density varies with ϕ in a manner similar to the conductivity, displaying a sharp rise around ϕ~0.08, followed by a more gradual increase. This is consistent with previous reports[19] on polymer-nanotube composites which show conductivity and carrier density follow nanotube content in very similar ways, coupled with relatively small increases in mobility. It addition, it contradicts our previous results which suggested mobility and carrier density both increase strongly with graphene content in 2D:2D composites.[21]

Here we found the carrier density data above the percolation threshold to be consistent with percolation-scaling:

$$p = p_0(\phi - \phi_c)^n \quad (10)$$

where p is the hole density and p_0, ϕ_c and n play similar roles to the parameters in Equation 3a. Equation 10 fits the data in Figure 5C (percolation plot in inset) very well, yielding p_0=2.3×10^{15} cm^{-2}, ϕ_c=0.09 and n=2.46 where we note that the latter two parameters are very close to those reported above.

It is worth noting that the value of p_0 obtained from the percolation fit is similar to values measured for graphene sheets.[56-57] This suggests the intriguing possibility that percolation of carrier density is more fundamental than percolation of conductivity because p_0 may represent a property of the conductive nanoparticles (here, the carrier density which in this case is probably set by environmental doping) rather than the conductive network. In contrast, σ_0 never represents the nanoparticle (i.e. in our case a graphene nanosheet or for example in nanotube-filled composites an individual nanotube) conductivity as it always includes the effect of inter-particle junctions.[58]

Conclusions

In conclusion, we have characterised the electrical properties of WS_2-graphene nano:nano composites formed by spray-coating networks of liquid-exfoliated nanosheets. In addition to performing conductivity measurements, through transistor analysis it was possible to extract information on mobility and carrier density as well as transistor properties, all as a function of graphene content. As expected, the composite network conductivity followed percolation theory with a percolation threshold of ~8 vol%. The on- and off-currents, measured during electrolytic gating, showed strong graphene content dependence, increasing sharply at the

percolation threshold. Interestingly, the loading dependence of both on- and off-currents are fitted well by percolation theory with the current flowing through the WS_2 network the only fit parameter which varied significantly under gate activation. The transistor measurements allowed us to estimate the network mobility. We found very slight (×3) mobility increase over the whole range of graphene content, suggesting only small differences between WS_2-WS_2, WS_2-graphene and graphene-graphene junction resistances. The dependence of the carrier density on graphene content was found by combining the network mobility with the network conductivity measured in the absence of electrolyte. We found the carrier density to increase sharply at the percolation threshold (8 vol%) before increasing by six orders of magnitude as the graphene content was increased. Interestingly, the carrier density followed percolation theory in a manner similar to the conductivity.

Methods

Ink preparation

Liquid phase exfoliation was the chosen method to produce the inks due to its versatility and production yield. All solvents used in this work are of HPLC grade. Pristine powders (WS_2 from Sigma Aldrich, CAS: 12138-09-9 Ref:243639, and graphene from Asbury, grade 3763) were poured in 80 mL of *N*-Methyl-2-pyrrolidone (NMP) at an initial concentration of C_0=40g/L and sonicated using a horn tip sonicator (Sonics Vibra-cell VCX-750 ultrasonic processor) at 60% amplitude, pulsed (6s on, 2s off) for an hour. The resulting dispersion was centrifuged at 3218 g in a Hettich Mikro 220R centrifuge for an hour. The supernatant was discarded and the sediment redispersed in 80 mL of fresh NMP and sonicated for 5 and 6 hours for WS_2 and graphene respectively, under the same conditions. After the exfoliation, the resulting dispersion is polydisperse in terms of flake's thickness (N) and lateral size (L).

The dispersions were homogenised with a two-step centrifugation protocol. The stock was centrifuged at a low centrifugation speed (500rpm) for an hour, in this step the unexfoliated material was removed. The supernatant was centrifuged at a higher speed (1000 rpm) and the resulting supernatant discarded. The sediment of this last centrifugation was redispersed in 50 mL IPA. A fraction of this last IPA dispersion was filtered and weighed, obtaining its concentration. If needed, the dispersion was diluted again to obtain concentrations below 1.5 g/L prior to spraying them.

Device fabrication

Al_2O_3-coated PET (Mitsubishi Paper Mills) was chosen as the substrate. The substrate was masked and placed below our sprayer (see SI) with ~30 cm separating substrate and spraygun and the N_2 gas flow was controlled by setting its pressure to 4 bars. Once the mask was removed, a set of sixteen 1×3×t mm^3 rectangular films of active material remained in the substrate. The thickness (t) of the film was measured with a mechanical profilometer. Gold interdigitated electrodes were deposited on top of the active material using shadow masks and a Temescal FC2000 metal evaporation system, defining a L×W×t (L=16mm, W=120 μm) transistor active channel. By depositing ~20 mL of WS_2 in IPA at 1.5 g/L concentration, ~1μm thick films were obtained. The thickness of all tested TFTs were measured by profilometry and found to be in the range 0.8-1.2 μm. The thickness of the channel has an impact on a number of parameters, such as mobility, conductivity, I_{on} and I_{off}. Mobility and conductivity were calculated using the measured thickness. I_{on} and I_{off} were rescaled to compensate for channel thickness variation and are presented as the values expected for a nominal thickness of 1 μm.

1-Ethyl-3-methylimidazolium bis(trifluoromethylsulfonyl)imide from Sigma Aldrich (EMIM-TFSI) was used as the ionic liquid. It was kept inside glovebox since first use and was degassed (80ºC overnight) before a drop was gently pipetted on top of the devices.

Electrical measurements

The electrical measurements were performed in a Janis probe station under high vacuum. This is to prevent water uptake in the ionic liquid, which would reduce the electrochemical window. To remove any water which may have been absorbed while placing the device into the chamber, the device was heated to 70 °C for 12 hr at ~10^{-5} mbar. A Keithley 2612A was used to perform the measurements. Scan rates of 10mV/s were used. The effect of scan rate on the I_{DS} values is shown in the SI.

Sixteen devices were printed for each volume fraction. Typically, all 16 functioned as expected but some sets of samples contained 1 or 2 non-functional devices which were discarded. The I_{ds}-V_G curves shown in Figure 2 are the curves for a single, representative device. However, all the data shown in Figures 3, 4 and 5 are the averages for a minimum of 14 devices.

Optical Spectroscopy

A Perkin Elmer Lambda 1050 spectrometer was used to measure the extinction spectra. The samples were diluted to a suitable optical density and measured using a quartz cuvette with an optical path length of 2 mm.

I_{DS} dynamics.

Measurements were performed as follows. V_{DS}=1V was applied once I_{DS} measurements began, 5 seconds later a -2.5 V potential step was applied to the gate electrode. In order to make a fair comparison Fig 4C shows the normalized I_{DS} (I_{DS}(t)-I_{off})/I_{max}, where I_{off} is the minimum I_{DS} value before the gate electrode is biased and I_{max} is the I_{DS} value once I_{DS} has reached the saturation plateau (present at long delay times).

Raman spectroscopy

Raman spectroscopy was performed on devices prior to IL deposition with a Horiba Jobin Yvon LabRAM HR800 with 532 nm excitation laser in air under ambient conditions. The Raman emission was collected by 100× objective lens (N.A. = 0.8) and dispersed by a 600 line/mm grating using 10 % of the laser power (~2 mW). 20 spectra, collected at different positions, were averaged to characterize each composite.

TEM Characterization

Bright-field transmission electron microscopy (TEM) was performed using a JOEL 2100 operated at 200 kV. Samples were diluted to a low concentration and drop cast onto a continuous carbon film TEM grid purchased from Agar Scientific. The TEM grid was placed on a filter membrane to wick away excess solvent and dried overnight at 150 °C in a vacuum oven. Statistical analysis was performed on the nanosheets dimensions by measuring the longest axis and defining it as the nanosheet length.

Supporting Information

An online document with supporting information that completes the data reported in this manuscript is available. The Supporting Information document includes data about annealing process, a detailed SEM imaging of the devices, cyclic voltammograms on different graphene loading levels, evolution of the volumetric capacitance with graphene loading level, and a scheme of the spraying set-up.

ACKNOWLEDGEMENTS: We acknowledge the European Research Council Advanced Grant (FUTURE-PRINT). Additional support was provided by Science Foundation Ireland (SFI/12/RC/2278) and the European Union under grant agreements n°785219 Graphene Flagship-core 2.

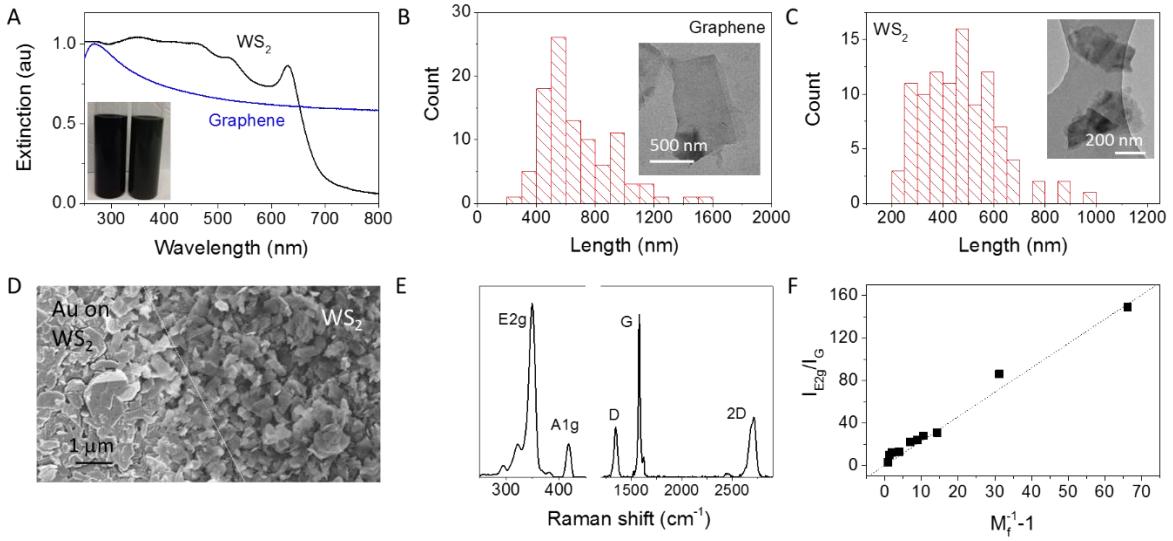

Figure 1. A, Inset) Photograph of size-selected graphene (left) and WS_2 (right) dispersions. Main panel) Extinction spectra of the dispersions shown in inset. B) Nanosheet length histogram of the graphene dispersion and (inset) a representative TEM image of a nanosheet. C) Nanosheet length histogram of the WS_2 dispersion and (inset) a representative TEM image of a nanosheet. D) SEM image of a WS_2 network following the deposition of gold electrodes with the bare WS_2 on the right and the gold-covered WS_2 on the left. E) Raman spectrum for WS_2-Gr composite (M_f=0.5). The two low frequency modes (E_{2g} and A_{1g} represent WS_2 while the D, G and 2D modes represents graphene. The portion of the spectrum containing the graphene modes has been magnified in intensity by ×2.5. F) A plot of the ratio of intensity of WS_2 to graphene peaks versus M_f^{-1} -1, where M_f is the graphene mass fraction. This plot is expected to be linear for a uniform mixture.

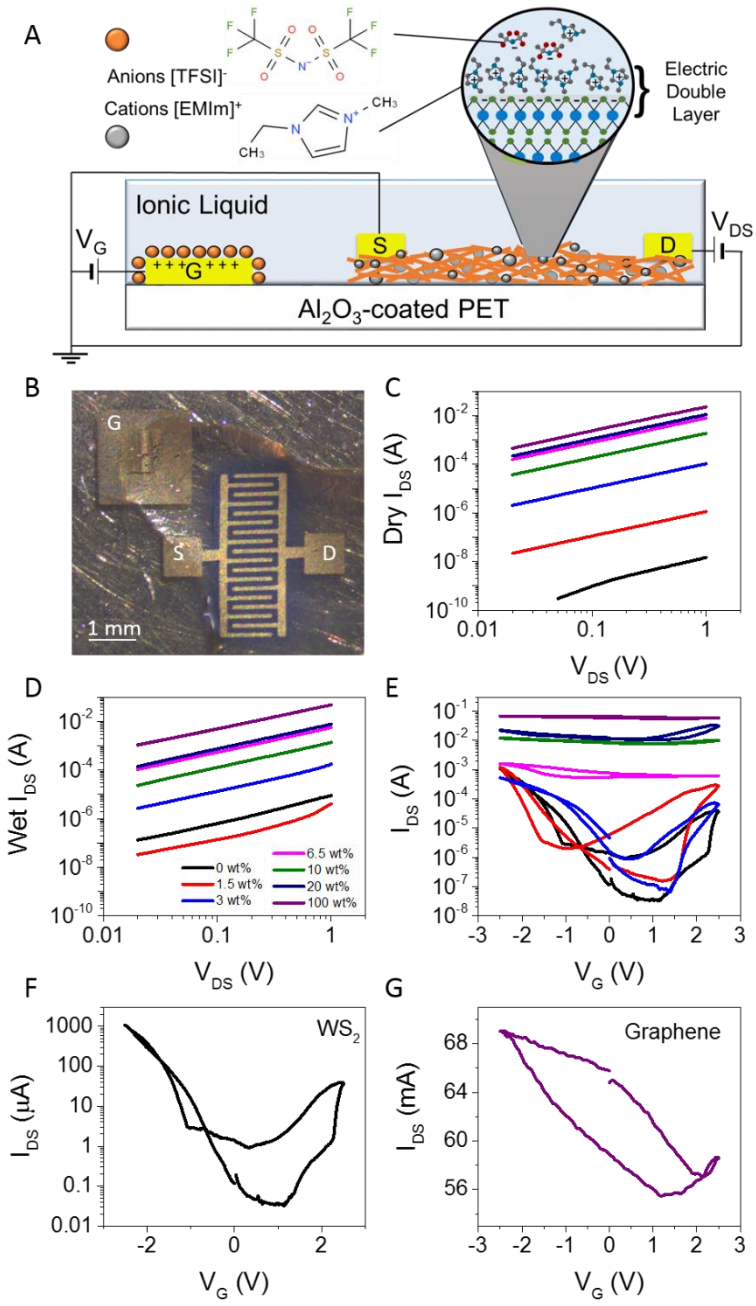

Figure 2. A) Schematic of an electrolytically gated TFT. B) Photograph of electrode array showing interdigitated source and drain (bottom right) and side gate (top left). C) Output curves before the ionic liquid is deposited on top of the devices ("dry"). D) Output curves after the ionic liquid is deposited on top of the devices ("wet"). E) Selected transfer curves for various graphene volume fractions. F-G) Transfer curves for (F) a purely WS_2 channel and (G) a purely graphene channel.

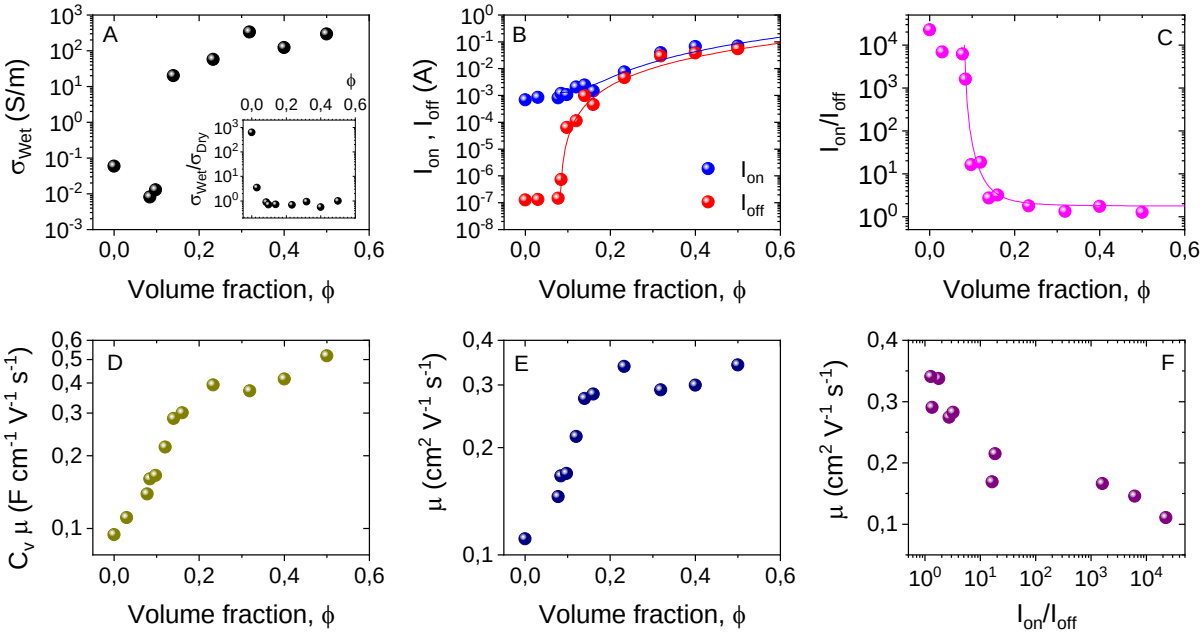

Figure 3. A) Conductivity in the presence of ionic liquid, σ_{Wet}, versus graphene volume fraction. As the porosity of the deposited film is 0.5 this is also the possible maximum graphene volume fraction. Inset: Ratio of the network conductivity before and after adding the ionic liquid. B) Dependence of the on-current (black) and off current (red) on graphene volume fraction. C) Dependence of the on:off current ratio on graphene volume fraction. D-E) Product of the volumetric capacitance and hole mobility (D) and resultant hole mobility (E) plotted versus graphene volume fraction. F) Mobility as a function of on:off ratio.

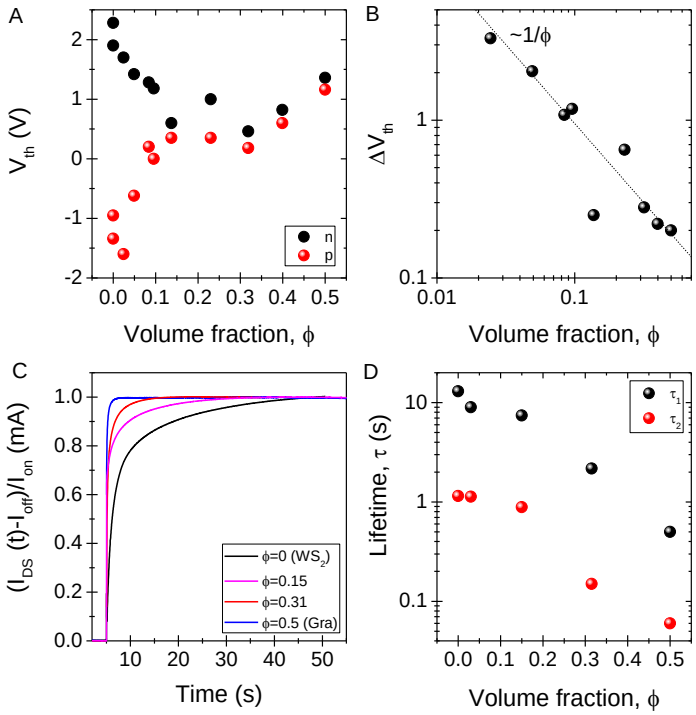

Figure 4. A) Electron and hole threshold voltage as a function of volume fraction. B) Reduction of ΔV_{th} as graphene volume-fraction increases. C) Response of $I_{DS}(t)$ to a step potential V_G= -2.5V. D) Lifetimes obtained from the bi-exponential fit of (C).

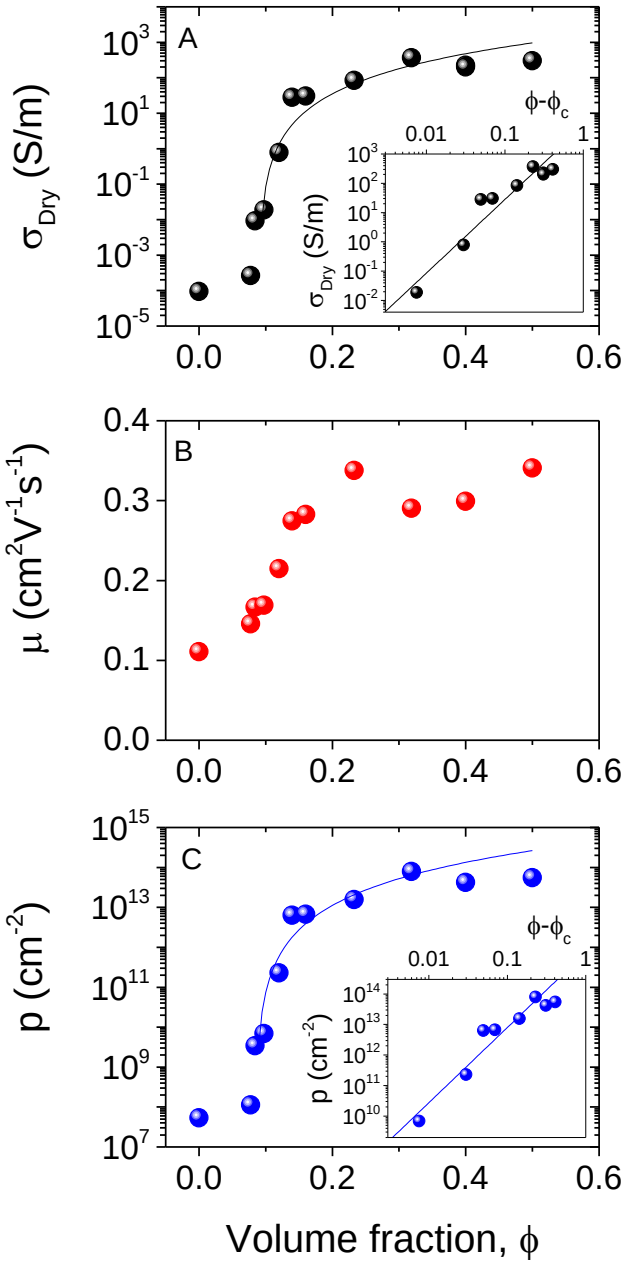

Figure 5. A) Conductivity of the WS_2 network (before the addition of ionic liquid), σ_{Dry}, versus graphene volume fraction. As the porosity of the deposited film is 0.5, the possible maximum graphene volume fraction is 0.5. B-C) Hole mobility (B, reproduced from Figure 3) and C) hole density (in the absence of ionic liquid) plotted versus graphene volume fraction. N.B. the calculation of carrier density relies on the assumption that the mobility is the same with and without ionic liquid.

1. Coleman, J. N.; Lotya, M.; O'Neill, A.; Bergin, S. D.; King, P. J.; Khan, U.; Young, K.; Gaucher, A.; De, S.; Smith, R. J.; Shvets, I. V.; Arora, S. K.; Stanton, G.; Kim, H. Y.; Lee, K.; Kim, G. T.; Duesberg, G. S.; Hallam, T.; Boland, J. J.; Wang, J. J.; Donegan, J. F.; Grunlan, J. C.; Moriarty, G.; Shmeliov, A.; Nicholls, R. J.; Perkins, J. M.; Grieveson, E. M.; Theuwissen, K.; McComb, D. W.; Nellist, P. D.; Nicolosi, V., Two-Dimensional Nanosheets Produced by Liquid Exfoliation of Layered Materials. *Science* **2011,** *331* (6017), 568-571.
2. Gabbett, C.; Boland, C. S.; Andrew Harvey; Vega-Mayoral, V.; Young, R. J.; Coleman, J. N., The Effect of Network Formation on the Mechanical Properties of 1d:2d Nano:Nano Composites. *Chem. Mater.* **2018,** *30* (15), 5245-5255.
3. Lota, G.; Fic, K.; Frackowiak, E., Carbon Nanotubes and Their Composites in Electrochemical Applications. *Energy Environ. Sci.* **2011,** *4* (5), 1592-1605.
4. Zhou, M.; Li, X. L.; Wang, B.; Zhang, Y. B.; Ning, J.; Xiao, Z. C.; Zhang, X. H.; Chang, Y. H.; Zhi, L. J., High-Performance Silicon Battery Anodes Enabled by Engineering Graphene Assemblies. *Nano Lett.* **2015,** *15* (9), 6222-6228.
5. Zhu, X. J.; Hu, J.; Dai, H. L.; Ding, L.; Jiang, L., Reduced Graphene Oxide and Nanosheet-Based Nickel Oxide Microsphere Composite as an Anode Material for Lithium Ion Battery. *Electrochim. Acta* **2012,** *64*, 23-28.
6. Chang, K.; Chen, W. X., L-Cysteine-Assisted Synthesis of Layered Mos_2/Graphene Composites with Excellent Electrochemical Performances for Lithium Ion Batteries. *ACS Nano* **2011,** *5* (6), 4720-4728.
7. David, L.; Bhandavat, R.; Singh, G., Mos_2/Graphene Composite Paper for Sodium-Ion Battery Electrodes. *ACS Nano* **2014,** *8* (2), 1759-1770.
8. Liu, H. M.; Yang, W. S., Ultralong Single Crystalline V_2O_5 Nanowire/Graphene Composite Fabricated by a Facile Green Approach and Its Lithium Storage Behavior. *Energy Environ. Sci.* **2011,** *4* (10), 4000-4008.
9. Zhang, S.; Zhu, L. X.; Song, H. H.; Chen, X. H.; Zhou, J. S., Enhanced Electrochemical Performance of Mno Nanowire/Graphene Composite During Cycling as the Anode Material for Lithium-Ion Batteries. *Nano Energy* **2014,** *10*, 172-180.
10. Liu, Y. P.; He, X. Y.; Hanlon, D.; Harvey, A.; Khan, U.; Li, Y. G.; Coleman, J. N., Electrical, Mechanical, and Capacity Percolation Leads to High-Performance Mos_2/Nanotube Composite Lithium Ion Battery Electrodes. *ACS Nano* **2016,** *10* (6), 5980-5990.
11. Wang, D. N.; Li, X. F.; Yang, J. L.; Wang, J. J.; Geng, D. S.; Li, R. Y.; Cai, M.; Sham, T. K.; Sun, X. L., Hierarchical Nanostructured Core-Shell Sn@C Nanoparticles Embedded in Graphene Nanosheets: Spectroscopic View and Their Application in Lithium Ion Batteries. *Phys. Chem. Chem. Phys.* **2013,** *15* (10), 3535-3542.
12. Zhou, J. S.; Ma, L. L.; Song, H. H.; Wu, B.; Chen, X. H., Durable High-Rate Performance of Cuo Hollow Nanoparticles/Graphene-Nanosheet Composite Anode Material for Lithium-Ion Batteries. *Electrochem. Commun.* **2011,** *13* (12), 1357-1360.
13. DiLeo, R. A.; Frisco, S.; Ganter, M. J.; Rogers, R. E.; Raffaelle, R. P.; Landi, B. J., Hybrid Germanium Nanoparticle-Single-Wall Carbon Nanotube Free-Standing Anodes for Lithium Ion Batteries. *J. Phys. Chem. C* **2011,** *115* (45), 22609-22614.
14. Kwak, W. J.; Lau, K. C.; Shin, C. D.; Amine, K.; Curtiss, L. A.; Sun, Y. K., A Mo2c/Carbon Nanotube Composite Cathode for Lithium-Oxygen Batteries with High Energy Efficiency and Long Cycle Life. *ACS Nano* **2015,** *9* (4), 4129-4137.
15. Jurewicz, I.; Fahimi, A.; Lyons, P. E.; Smith, R. J.; Cann, M.; Large, M. L.; Tian, M. W.; Coleman, J. N.; Dalton, A. B., Insulator-Conductor Type Transitions in Graphene-

Modified Silver Nanowire Networks: A Route to Inexpensive Transparent Conductors. *Adv. Func. Mater.* **2014,** *24* (48), 7580-7587.
16. Peng, S. J.; Li, L. L.; Han, X. P.; Sun, W. P.; Srinivasan, M.; Mhaisalkar, S. G.; Cheng, F. Y.; Yan, Q. Y.; Chen, J.; Ramakrishna, S., Cobalt Sulfide Nanosheet/Graphene/Carbon Nanotube Nanocomposites as Flexible Electrodes for Hydrogen Evolution. *Angew. Chem.,Int. Ed.* **2014,** *53* (46), 12594-12599.
17. McAteer, D.; Gholamvand, Z.; McEvoy, N.; Harvey, A.; O'Malley, E.; Duesberg, G. S.; Coleman, J. N., Thickness Dependence and Percolation Scaling of Hydrogen Production Rate in Mos_2 Nanosheet and Nanosheet-Carbon Nanotube Composite Catalytic Electrodes. *ACS Nano* **2016,** *10* (1), 672-683.
18. Atkin, P.; Daeneke, T.; Wang, Y.; Carey, B. J.; Berean, K. J.; Clark, R. M.; Ou, J. Z.; Trinchi, A.; Cole, I. S.; Kalantar-Zadeh, K., 2d Ws_2/Carbon Dot Hybrids with Enhanced Photocatalytic Activity. *J. Mater. Chem.* **2016,** *4*, 13563-13571.
19. Tan, H.-x.; Xu, X.-c., Conductive Properties and Mechanisms of Different Polymers Doped by Carbon Nanotube/Polypyrrole 1d Hybrid Nanotubes. *RSC Adv* **2015,** *5* (75), 61383-61389.
20. Murthy, D. V. B.; Subramanian, V.; Sundaray, B.; Natarajan, T. S., Microwave Hall Mobility Studies on Polymer-Single Walled Carbon Nanotube Composite Fibers. *Appl. Phys. Lett.* **2008,** *92* (22).
21. Kelly, A. G.; Murphy, C.; Vega-Mayoral, V.; Andrew Harvey; Esmaeily, A.; Toby Hallam; McCloskey, D.; Coleman, J. N., Tuneable Photoconductivity and Mobility Enhancement in Printed Mos_2/Graphene Composites. *2D Mater* **2017,** *4* (4), 041006.
22. Carey, T.; Cacovich, S.; Divitini, G.; Ren, J. S.; Mansouri, A.; Kim, J. M.; Wang, C. X.; Ducati, C.; Sordan, R.; Torrisi, F., Fully Inkjet-Printed Two-Dimensional Material Field-Effect Heterojunctions for Wearable and Textile Electronics. *Nat Commun* **2017,** *8*, 11.
23. Hu, G. H.; Albrow-Owen, T.; Jin, X. X.; Ali, A.; Hu, Y. W.; Howe, R. C. T.; Shehzad, K.; Yang, Z. Y.; Zhu, X. K.; Woodward, R. I.; Wu, T. C.; Jussila, H.; Wu, J. B.; Peng, P.; Tan, P. H.; Sun, Z. P.; Kelleher, E. J. R.; Zhang, M.; Xu, Y.; Hasan, T., Black Phosphorus Ink Formulation for Inkjet Printing of Optoelectronics and Photonics. *Nat Commun* **2017,** *8*.
24. Li, J. T.; Ye, F.; Vaziri, S.; Muhammed, M.; Lemme, M. C.; Ostling, M., Efficient Inkjet Printing of Graphene. *Adv. Mater.* **2013,** *25* (29), 3985-3992.
25. McManus, D.; Vranic, S.; Withers, F.; Sanchez-Romaguera, V.; Macucci, M.; Yang, H.; Sorrentino, R.; Parvez, K.; Son, S.-K.; Iannaccone, G.; Kostarelos, K.; Fiori, G.; Casiraghi, C., Water-Based and Biocompatible 2d Crystal Inks for All-Inkjet-Printed Heterostructures. *Nat. Nanotechnol.* **2017,** *12* (4), 343-350.
26. Torrisi, F.; Hasan, T.; Wu, W.; Sun, Z.; Lombardo, A.; Kulmala, T. S.; Hsieh, G.-W.; Jung, S.; Bonaccorso, F.; Paul, P. J.; Chu, D.; Ferrari, A. C., Inkjet-Printed Graphene Electronics. *ACS Nano* **2012,** *6* (4), 2992-3006.
27. Kelly, A. G.; Hallam, T.; Backes, C.; Harvey, A.; Esmaeily, A. S.; Godwin, I.; Coelho, J.; Nicolosi, V.; Lauth, J.; Kulkarni, A.; Kinge, S.; Siebbeles, L. D. A.; Duesberg, G. S.; Coleman, J. N., All-Printed Thin-Film Transistors from Networks of Liquid-Exfoliated Nanosheets. *Science* **2017,** *356*, 69-72.
28. Niu, L. Y.; Coleman, J. N.; Zhang, H.; Shin, H.; Chhowalla, M.; Zheng, Z. J., Production of Two-Dimensional Nanomaterials Via Liquid-Based Direct Exfoliation. *Small* **2016,** *12* (3), 272-293.
29. Backes, C.; Szydłowska, B. M.; Harvey, A.; Yuan, S.; Vega-Mayoral, V.; Davies, B. R.; Zhao, P.-l.; Hanlon, D.; Santos, E. J. G.; Katsnelson, M. I.; Blau, W. J.; Gadermaier, C.; Coleman, J. N., Production of Highly Monolayer Enriched Dispersions of Liquid-Exfoliated Nanosheets by Liquid Cascade Centrifugation. *ACS Nano* **2016,** *10* (1), 1589-1601.

30. Vega-Mayoral, V.; Vella, D.; Borzda, T.; Prijatelj, M.; Tempra, I.; Pogna, E. A. A.; Dal Conte, S.; Topolovsek, P.; Vujicic, N.; Cerullo, G.; Mihailovic, D.; Gadermaier, C., Exciton and Charge Carrier Dynamics in Few-Layer Ws_2. *Nanoscale* **2016,** *8*, 5428-5434.
31. Mak, K. F.; Lee, C.; Hone, J.; Shan, J.; Heinz, T. F., Atomically Thin Mos_2: A New Direct-Gap Semiconductor. *Phys. Rev. Lett.* **2010,** *105* (13), 136805.
32. Kravets, V. G.; Grigorenko, A. N.; Nair, R. R.; Blake, P.; Anissimova, S.; Novoselov, K. S.; Geim, A. K., Spectroscopic Ellipsometry of Graphene and an Exciton-Shifted Van Hove Peak in Absorption. *Phys. Rev. B* **2010,** *81*, 155413.
33. Backes, C.; Paton, K. R.; Hanlon, D.; Yuan, S.; Katsnelson, M. I.; Houston, J.; Smith, R. J.; McCloskey, D.; Donegan, J. F.; Coleman, J. N., Spectroscopic Metrics Allow in Situ Measurement of Mean Size and Thickness of Liquid-Exfoliated Few-Layer Graphene Nanosheets. *Nanoscale* **2016,** *8* (7), 4311-4323.
34. Leea, K.-M.; Hsub, C.-Y.; Chiuc, W.-H.; Tsuia, M.-C.; Tunga, Y.-L.; Tsaia, S.-Y.; Hob, K.-C., Dye-Sensitized Solar Cells with a Micro-Porous Tio_2 Electrode and Gel Polymer Electrolytes Prepared by in Situ Cross-Link Reaction. *Sol. Energy Mater Sol. Cells* **2009,** *2009*, 2003-2007.
35. Atta, N. F.; Gawad, S. A. A.; El-Ads, E. H.; El-Gohary, A. R. M.; Galal, A., A New Strategy for Nadh Sensing Using Ionic Liquid Crystals-Carbon Nanotubes/Nano-Magnetite Composite Platform. *Sensor Actuat B-Chem* **2017,** *251*, 65-73.
36. Cunningham, G.; Lotya, M.; McEvoy, N.; Duesberg, G. S.; van der Schootcd, P.; Coleman, J. N., Percolation Scaling in Composites of Exfoliated Mos_2 Filled with Nanotubes and Graphene. *Nanoscale* **2012,** *4*, 6260 - 6264.
37. Gholamvand, Z.; McAteer, D.; Harvey, A.; Backes, C.; Coleman, J. N., Electrochemical Applications of Two-Dimensional Nanosheets: The Effect of Nanosheet Length and Thickness. *Chem. Mater.* **2016,** *28* (8), 2641-2651.
38. McLachlan, D. S.; Sauti, G., The Ac and Dc Conductivity of Nanocomposites. *J. Nanomater.* **2007**.
39. Ling, Z.; Harvey, A.; McAteer, D.; Godwin, I. J.; Szydlowska, B.; Griffin, A.; Vega-Mayoral, V.; Song, Y. C.; Seral-Ascaso, A.; Nicolosi, V.; Coleman, J., Quantifying the Role of Nanotubes in Nano:Nano Composite Supercapacitor Electrodes. *Adv. Energy Mater.* **2018,** *8* (8).
40. Yu, X. Y.; Prevot, M. S.; Sivula, K., Multiflake Thin Film Electronic Devices of Solution Processed 2d Mos2 Enabled by Sonopolymer Assisted Exfoliation and Surface Modification. *Chem. Mater.* **2014,** *26* (20), 5892-5899.
41. De, S.; Coleman, J. N., Are There Fundamental Limitations on the Sheet Resistance and Transmittance of Thin Graphene Films? *ACS Nano* **2010,** *4* (5), 2713-2720.
42. Lin, Z.; Liu, Y.; Halim, U.; Ding, M.; Liu, Y.; Wang, Y.; Jia, C.; Chen, P.; Duan, X.; Wang, C.; Song, F.; Li, M.; Wan, C.; Huang, Y.; Duan, X., Solution-Processable 2d Semiconductors for High-Performance Large-Area Electronics. *Nature* **2018,** *562*, 254-258.
43. Braga, D.; Gutierrez-Lezama, I.; Berger, H.; Morpurgo, A. F., Quantitative Determination of the Band Gap of Ws_2 with Ambipolar Ionic Liquid-Gated Transistors. *Nano Lett.* **2012,** *12*, 5218−5223.
44. Gutiérrez-Lezama, I.; Reddy, B. A.; Ubrig, N.; Morpurgo, A. F., Electroluminescence from Indirect Band Gap Semiconductor Res_2. *2D Mater* **2016,** *3*, 045016.
45. Chernikov, A.; Berkelbach, T. C.; Hill, H. M.; Rigosi, A.; Li, v.; Aslan, O. B.; Reichman, D. R.; Hybertsen, M. S.; Heinz, T. F., Exciton Binding Energy and Nonhydrogenic Rydberg Series in Monolayer Ws_2. *Phys. Rev. Lett.* **2014,** *113*, 076802.
46. Zhu, B.; Chen, X.; Cui, X., Exciton Binding Energy of Monolayer Ws_2. *Sci. Rep.* **2015,** *5*, 9218.

47. Ye, Z.; Cao, T.; O'Brien, K.; Zhu, H.; Yin, X.; Wang, Y.; Louie, S. G.; Zhang, X., Probing Excitonic Dark States in Single-Layer Tungsten Disulphide. *Nature* **2014,** *513*, 214-218.
48. Hill, H. M.; Rigosi, A.; Roquelet, C.; Chernikov, A.; Berkelbach, T. C.; Reichman, D. R.; Hybertsen, M. S.; Brus, L. E.; Heinz, T. F., Observation of Excitonic Rydberg States in Monolayer Mos_2 and Ws_2 by Photoluminescence Excitation Spectroscopy. *Nano Lett.* **2015,** *15* (5), 2992-2997.
49. Kim, S. H.; Hong, K.; Xie, W.; Lee, K. H.; Zhang, S. P.; Lodge, T. P.; Frisbie, C. D., Electrolyte-Gated Transistors for Organic and Printed Electronics. *Adv. Mater.* **2013,** *25* (13), 1822-1846.
50. Gebbie, M. A.; Valtiner, M.; Banquy, X.; Fox, E. T.; Henderson, W. A.; Israelachvili, J. N., Ionic Liquids Behave as Dilute Electrolyte Solutions. *PNAS* **2013,** *110* (24), 9674-9679.
51. Stankovich, S.; Dikin, D. A.; Dommett, G. H. B.; Kohlhaas, K. M.; Zimney, E. J.; Stach, E. A.; Piner, R. D.; Nguyen, S. T.; Ruoff, R. S., Graphene-Based Composite Materials. *Nature* **2006,** *442* (7100), 282-286.
52. Zhang, B.; Yu, Y.; Liu, Y. S.; Huang, Z. D.; He, Y. B.; Kim, J. K., Percolation Threshold of Graphene Nanosheets as Conductive Additives in Li4ti5o12 Anodes of Li-Ion Batteries. *Nanoscale* **2013,** *5* (5), 2100-2106.
53. Uesugi, E.; Goto, H.; Eguchi, R.; Fujiwara, A.; Kubozono, Y., Electric Double-Layer Capacitance between an Ionic Liquid and Few-Layer Graphene. *Sci. Rep.* **2013,** *3*, 1595.
54. Nirmalraj, P. N.; Lutz, T.; Kumar, S.; Duesberg, G. S.; Boland, J. J., Nanoscale Mapping of Electrical Resistivity and Connectivity in Graphene Strips and Networks. *Nano Lett.* **2011,** *11* (1), 16-22.
55. Nirmalraj, P. N.; Lyons, P. E.; De, S.; Coleman, J. N.; Boland, J. J., Electrical Connectivity in Single-Walled Carbon Nanotube Networks. *Nano Lett.* **2009,** *9* (11), 3890-3895.
56. Pachoud, A.; Jaiswal, M.; Ang, P. K.; P., L.; Özyilmaz, B., Graphene Transport at High Carrier Densities Using a Polymer Electrolyte Gate. *EPL (Europhysics Letters)* **2010,** *92* (2), 27001.
57. Fang, T.; Konar, A.; Xing, H.; Jena, D., Carrier Statistics and Quantum Capacitance of Graphene Sheets and Ribbons. *Appl. Phys. Lett.* **2007,** *91*, 092109.
58. Foygel, M.; Morris, R. D.; Anez, D.; French, S.; Sobolev, V. L., Theoretical and Computational Studies of Carbon Nanotube Composites and Suspensions: Electrical and Thermal Conductivity. *Phys. Rev. B* **2005,** *71* (10).

Table of contents